CMS Physics Analysis Summary

Contact: cms-pag-conveners-top@cern.ch 2019/03/07

Constraining the top quark Yukawa coupling from $t\bar{t}$ differential cross sections in the lepton+jets final state in proton-proton collisions at $\sqrt{s} = 13$ TeV

The CMS Collaboration

Abstract

A measurement of the top quark Yukawa coupling from the top quark-antiquark ($t\bar{t}$) differential production cross sections in proton-proton collisions with the lepton+jets channel is presented. Corrections due to electroweak bosons exchange, including the Higgs boson, between the final state top quarks can produce large distortions of differential distributions near the energy threshold of top quark pair production. Therefore precise measurements of these distributions are sensitive to the Yukawa coupling. This analysis is based on data collected by the CMS experiment at the LHC at $\sqrt{s} = 13$ TeV corresponding to an integrated luminosity of 35.8 fb^{-1}. Top quark events are reconstructed with at least three jets in the final state. A novel technique is introduced to reconstruct the $t\bar{t}$ system for events with one missing jet. This technique enhances the experimental sensitivity in the low invariant mass region, $M_{t\bar{t}}$. The data yields in $M_{t\bar{t}}$, the rapidity difference $|y_t - y_{\bar{t}}|$, and the number of reconstructed jets are compared with distributions representing different Yukawa couplings. These comparisons are used to extract an upper limit on the top quark Yukawa coupling of 1.67 (1.62 expected) at 95% confidence level.

1 Introduction

Precise measurements of the top quark pair ($t\bar{t}$) production cross section and the decay properties of the top quark provide crucial information to test the standard model (SM) and to search for new phenomena. Recent calculations provide next-to-next-to-leading-order (NNLO) predictions within the framework of perturbative QCD for the $t\bar{t}$ production cross section [1, 2]. Weak force mediated corrections only affect the cross section at loop-induced order $\alpha_s^2\alpha_{\text{weak}}$ (Fig. 1), so they make a small contribution to the total cross section and are not implemented in the Monte Carlo (MC) event generators. However, in kinematic regions with large momentum transfer, weak corrections become large and may lead to large distortions of differential distributions. In addition, it has been shown that in the threshold region, which corresponds to kinematic regions with small relative velocity between the top quark and antiquark, the $t\bar{t}$ cross section is sensitive to the top quark Yukawa coupling through weak force mediated corrections [3]. For example, doubling the Yukawa coupling would lead to a change in the cross section of about 9%, which is larger than the current experimental sensitivity of around 6% [4].

Figure 1: Example diagrams for gluon-induced process of $t\bar{t}$ production and the virtual corrections. Γ stands for all contributions from the gauge boson, Goldstone boson and Higgs boson exchanges.

A detailed study of the differential $t\bar{t}$ kinematic properties close to the production threshold could, therefore, determine the value of top quark Yukawa coupling. In this analysis, we define Y_t as the ratio of the top quark Yukawa coupling to its SM predicted value. We calculate the electroweak correction factors for different values of Y_t using HATHOR [5] and apply them at the parton level to the existing $t\bar{t}$ simulated samples. From these modified simulations, we obtain distributions at detector level that can be directly compared to the data. The Yukawa coupling is extracted from the distributions of the invariant mass of the top quark pair, $M_{t\bar{t}}$, and the rapidity difference between the top quark and antiquark, $\Delta y_{t\bar{t}} = y_t - y_{\bar{t}}$, for different jet multiplicities. The analysis covers the phase space from the production threshold in $M_{t\bar{t}}$ (which is ≈200 GeV at the detector level) to 2 TeV, and from 0 to 6 in $|\Delta y_{t\bar{t}}|$. Low $M_{t\bar{t}}$ and small $|\Delta y_{t\bar{t}}|$ regions are the most sensitive to Y_t.

Top quarks decay almost exclusively through $t \to Wb$ and the final topology depends on the W bosons' decays. When one W boson decays leptonically and the other decays hadronically $t\bar{t} \to W^+b\,W^-\bar{b} \to \ell^+\nu b\,q\bar{q}'\bar{b}$, the final state at leading order consists of an isolated lepton (electron or muon in this analysis), missing transverse momentum (from the neutrino), and four jets (from two b quarks and two light quarks). This final state has a sizable branching ratio (34%), small backgrounds, and allows for the kinematic reconstruction of the original top candidates. This analysis follows the same methodology employed in Ref. [6] and introduces a novel algorithm to reconstruct the $t\bar{t}$ pair when only three jets are present.

The outline of this note is as follows. In Sec. 2, the method of implementing electroweak corrections in simulated samples and the variables sensitive to the top Yukawa coupling are introduced. The data and simulated samples used for the analysis are described in Sec. 3. Event selection criteria are explained in Sec. 4. The algorithm used to reconstruct $t\bar{t}$ events is described in Sec. 5. Details on background estimation and the event yields are described in Sec. 6

and Sec. 7. The statistical methodologies and the systematic uncertainties are described in Sec. 8 and Sec. 9. In Sec. 10, the results are presented, including the limits on the Yukawa coupling.

2 Electroweak correction

Electroweak (EW) corrections to the $\mathrm{t\bar{t}}$ production cross section were originally calculated [7] before the top quark discovery, and were found to have a very small effect on the total cross section. However, they can have a sizable impact on differential distributions and the top quark charge asymmetry. There is no interference term of order $\alpha_s\alpha$ between the lowest-order strong force mediated and neutral current amplitudes in the quark-induced processes. Electroweak corrections start entering the cross section at loop-induced order $\alpha_s^2\alpha$, as shown in Fig. 1. A majority of EW corrections do not depend on the top quark Yukawa coupling. Contributions linear in Y_t, which arise from the production of an intermediate s-channel Higgs boson through a closed b-quark loop, can be ignored due to the small b-quark mass. Higgs boson exchange between the final state top quark and antiquark, which involves two $\mathrm{Ht\bar{t}}$ vertices, as shown in Fig. 1, leads to a quadratic dependence of the cross section on the top quark Yukawa coupling.

HATHOR [5] calculates the partonic cross section value, including the EW corrections at leading order $\mathcal{O}(\alpha_s^2\alpha)$ for a given $M_{\mathrm{t\bar{t}}}$ and $\Delta y_{\mathrm{t\bar{t}}}$. The mass of the top quark is fixed at $m_\mathrm{t} = 172.5\,\mathrm{GeV}$, and is treated as a source of systematic uncertainty. We use HATHOR to extract a two-dimensional correction factor that contains the ratio of the $\mathrm{t\bar{t}}$ production cross section with EW corrections over the leading-order production cross section in bins of $M_{\mathrm{t\bar{t}}}$ and $\Delta y_{\mathrm{t\bar{t}}}$. This is done for different hypothesized values Y_t. We then apply this correction factor at the parton level to each $\mathrm{t\bar{t}}$ event simulated with POWHEG [8–11]. Figure 2 shows the relative EW correction on the next-to-leading-order (NLO) QCD production cross section as a function of $M_{\mathrm{t\bar{t}}}$ and $\Delta y_{\mathrm{t\bar{t}}}$ for different values of Y_t. Non-SM Y_t values lead to large distortions in the $M_{\mathrm{t\bar{t}}}$ and $\Delta y_{\mathrm{t\bar{t}}}$ spectra. However, in the distributions at detector level the experimental resolutions and the systematic uncertainties, which are especially significant in the low $M_{\mathrm{t\bar{t}}}$ region, can reduce the sensitivity to this effect.

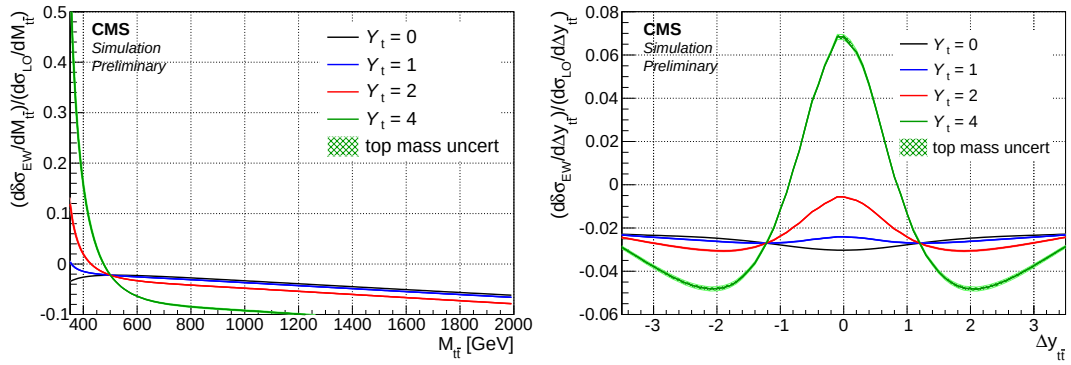

Figure 2: The dependence of the ratio of EW correction over the leading-order production cross section on the sensitive kinematic variables $M_{\mathrm{t\bar{t}}}$ and $\Delta y_{\mathrm{t\bar{t}}}$ for different values of Yukawa coupling, as evaluated with HATHOR [5]. The lines contain an uncertainty band derived from the dependence of the EW correction on the top quark mass varied by $\pm 1\,\mathrm{GeV}$. The effect of the top quark mass is very small at the parton level and not visible in the scale of the plot.

3 Data set and modeling

Events are taken from certified runs, for which a good performance and full functionality of the CMS detector is ensured. These runs correspond to an integrated luminosity of $35.8\,\mathrm{fb}^{-1}$.

Events are selected if they pass single lepton triggers. These require a transverse momentum $p_T > 27\,\text{GeV}$ for electrons and $p_T > 24\,\text{GeV}$ for muons, both within pseudorapidity $|\eta| < 2.4$, as well as various quality and isolation criteria.

The MC event generator POWHEG [8–11] (v2) is used to simulate $t\bar{t}$ events. It calculates up to NLO QCD matrix elements and uses PYTHIA8 [12, 13] (v8.205) Tune CUETP8M2T4 [14] for the parton shower simulations. The default parametrization of the parton distribution functions (PDFs) used in all simulations is NNPDF3.0 [15]. A top quark mass of 172.5 GeV is used. When compared to the data, the simulation is normalized to an inclusive $t\bar{t}$ production cross section of 832^{+40}_{-46} pb [16]. This value is calculated with NNLO accuracy, including the resummation of next-to-next-to-leading-logarithmic (NNLL) soft gluon terms. The presented uncertainty is due to the choice of hadronization/factorization scales and PDF.

The background processes are modeled using the same techniques. The MG5_aMC@NLO generator [17] is used to simulate W boson and Drell–Yan (DY) production in association with jets and t-channel production of single top quark. The POWHEG generator is used to simulate a single top quark produced in association with a W boson (tW) and PYTHIA8 is used for multijet production. In all cases, the parton shower and the hadronization are simulated by PYTHIA8. The W boson and DY backgrounds are normalized to their NNLO cross sections calculated with FEWZ [18]. The single top quark processes are normalized to NLO calculations [19, 20], and the multijet simulation is normalized to the leading-order (LO) calculation from PYTHIA8 [13]. The multijet simulation is later rescaled using control data sets.

The detector response is simulated using GEANT4 [21]. The same algorithms that are applied to the collider data are used to reconstruct the simulated data. Multiple proton-proton interactions per bunch crossing (pileup) are included in the simulation. To correct the simulation to be in agreement with the pileup conditions observed during the data taking, the average number of pileup events per bunch crossing is calculated for the measured instantaneous luminosity. The simulated events are weighted, depending on their number of pileup interactions, to reproduce the measured pileup distribution.

4 Event reconstruction and selection

Jets are reconstructed from PF particle candidates, clustered by the anti-k_T algorithm [22, 23] with a distance parameter $R = 0.4$. Jet momentum is determined as the vectorial sum of all PF candidate momenta in the jet. An offset correction is applied to jet energies to take into account the contribution from pileup within the same or nearby bunch crossings. Jet energy corrections are derived from simulation, and are improved with in situ measurements of the energy balance in dijet and photon+jet events [24, 25]. Additional selection criteria are applied to each event to remove spurious jet-like features originating from isolated noise patterns in certain HCAL regions.

Jets are identified as originating from b quarks using the combined secondary vertex algorithm (CSV) [26]. Data samples are used to measure the probability of correctly identifying jets as originating from b quarks (b tagging efficiency), and the probability of misidentifying jets originating from light-flavor partons (u, d, s quarks or gluons) or a charm quark as a b-tagged jet (the light-flavor and charm mistag probabilities) [27]. A working point is employed that yields a b tagging efficiency of 63%, and charm and light-flavor mistag probabilities of approximately 12% and 2%, respectively (around 3% in total), for jets with p_T typical of $t\bar{t}$ events.

The missing transverse momentum, $\vec{p}_T^{\,\text{miss}}$, is calculated as the negative vector sum of the trans-

verse momenta of all PF candidates in an event. Its magnitude is referred to as $p_{\mathrm{T}}^{\mathrm{miss}}$.

Candidate signal events are defined by the presence of a muon or an electron that is isolated from other activity in the event, specifically jets, and missing transverse momentum associated with a neutrino. The isolation variables exclude the contributions from the physics object itself and pileup events. The efficiencies of lepton identification and selection criteria are derived using a tag-and-probe method in p_{T} and η regions [28].

To reduce the background contributions and to optimize the $\mathrm{t\bar{t}}$ reconstruction, additional, more stringent, requirements on the events are imposed. Only events with exactly one muon or electron with $p_{\mathrm{T}} > 30\,\mathrm{GeV}$ and $|\eta| < 2.4$ are selected. No additional muons or electrons with $p_{\mathrm{T}} > 15\,\mathrm{GeV}$ and $|\eta| < 2.4$ are allowed. At least three jets with $p_{\mathrm{T}} > 30\,\mathrm{GeV}$ and $|\eta| < 2.4$ are required, and at least two of them must be b-tagged. The W transverse mass, defined by $M_{\mathrm{T}}^2(W) = 2(E_{\mathrm{T}}^{\ell} p_{\mathrm{T}}^{\mathrm{miss}} - \vec{p}_{\mathrm{T}}^{\,\ell} \cdot \vec{p}_{\mathrm{T}}^{\,\mathrm{miss}})$, is required to be less than 140 GeV, where E_{T}^{ℓ} and $\vec{p}_{\mathrm{T}}^{\,\ell}$ refer to the transverse energy and transverse momentum for the lepton. For $\mathrm{t\bar{t}}$ events with three jets in the final state, the p_{T} of the leading b-tagged jet is required to be greater than 50 GeV.

5 Reconstruction of the top quark-antiquark system

The goal of reconstructing $\mathrm{t\bar{t}}$ events is to determine the top quark/antiquark four-momenta. For this, it is necessary to correctly match the final state objects to the originating top quarks and their decay products. We always assume that the two b-tagged jets with the highest CSV values are associated with the two b quarks from $\mathrm{t\bar{t}}$ decays. For each event, we test all possible assignments of jets to quarks from the $\mathrm{t\bar{t}}$ decay consistent with this requirement and select the one with the highest value of a likelihood discriminant constructed based on the available information.

The first step in building this likelihood discriminant is to reconstruct the neutrino four-momentum p_ν based on the measured $\vec{p}_{\mathrm{T}}^{\,\mathrm{miss}}$, the lepton momentum p_ℓ and the momentum p_{b_ℓ} of the jet associated to the b quark from the top quark decay. The Neutrino Solver algorithm [29] uses a geometric approach to find all possible solutions for the neutrino momentum based on the two mass constraints $(p_\nu + p_\ell)^2 = m_{\mathrm{W}}^2$ and $(p_\nu + p_\ell + p_{\mathrm{b}_\ell})^2 = m_{\mathrm{t}}^2$. Each equation describes an ellipsoid in the three-dimensional neutrino momentum space. The intersection of these two ellipsoids is usually an ellipse. We select p_ν as the point on the ellipse for which the distance $D_{\nu,\mathrm{min}}$ between the ellipse projection onto the transverse plane $(p_{\nu x}, p_{\nu y})$ and the measured $\vec{p}_{\mathrm{T}}^{\,\mathrm{miss}}$ is minimal. The algorithm leads to a unique solution for the longitudinal neutrino momentum and an improved resolution for the transverse component. The minimum distance $D_{\nu,\mathrm{min}}$ is also used to identify the correct b jet in the leptonic top quark decay, b_ℓ. When the invariant mass of the lepton and b_ℓ candidate is above m_{t}, no solution can be found and this jet assignment is discarded. If both b_ℓ candidates fail this requirement, then the event is categorized as not reconstructible.

5.1 Reconstruction of events with at least four jets

The likelihood discriminant for events with at least four reconstructed jets is built to minimize the calculated $D_{\nu,\mathrm{min}}$ and to simultaneously ensure that the invariant mass of the two jets hypothesized to originate from W boson decay (m_2) is consistent with the W boson mass and that the invariant mass of the three jets hypothesized to originate from the hadronically decaying top quark (m_3) is consistent with the top quark mass. The likelihood discriminant is defined as λ_4 (the label 4 refers to the requirement of at least four jets):

$$-\ln(\lambda_4) = -\ln(P_{\mathrm{m}}(m_2, m_3)) - \ln(P_\nu(D_{\nu,\mathrm{min}})), \quad (1)$$

where P_{m} is the two-dimensional probability distribution to correctly reconstruct the W boson and top quark invariant masses.

The probability P_ν describes the distribution of $D_{\nu,\mathrm{min}}$ for a correctly selected b_ℓ. On average, the distance $D_{\nu,\mathrm{min}}$ for a correctly selected b_ℓ is smaller and has a lower tail compared to the distance obtained for other jets. Jet assignments with values of $D_{\nu,\mathrm{min}} > 150$ GeV are rejected since they are very unlikely to originate from a correct b_ℓ association. The distributions for P_{m}, $D_{\nu,\mathrm{min}}$, and λ_4 can be found in Figs. 2 and 4 of Ref. [6].

The efficiency of the reconstruction algorithm is defined as the probability that the most likely assignment, as identified by the largest value of λ_4, is the correct one, given that all decay products from the $\mathrm{t\bar{t}}$ decay are reconstructed and selected. Since the number of possible assignments increases drastically with the number of jets, it is more likely to select a wrong assignment if there are additional jets. The algorithm identifies the correct assignment in around 84% of the four-jet events, 69% in five-jet events, and 53% in six-jet events.

5.2 Reconstruction of events with one missing jet

The most sensitive region of phase space to probe the size of the top Yukawa coupling is at the threshold of $\mathrm{t\bar{t}}$ production. However, the efficiency for selecting $\mathrm{t\bar{t}}$ events in this region is rather low, since one or more quarks from $\mathrm{t\bar{t}}$ decay are likely to have p_{T} or η outside of the selection thresholds resulting in a missing jet. To mitigate this effect, we developed an algorithm of $\mathrm{t\bar{t}}$ reconstruction for events with one missing jet [30].

We require that there are exactly three jets in the event with at least two of them b-tagged. We assume that the two jets with the highest value of the CSV discriminator are associated with b quarks from $\mathrm{t\bar{t}}$ decays. In 93% of the selected three-jet $\mathrm{t\bar{t}}$ events, the missing jet is associated with the quark from the W decay. The remaining two-fold ambiguity is in the assignment of the b-tagged jets: which one originates from the hadronic top quark decay and which one from the leptonic top quark decay. For each of the two possible b-jet assignments, the algorithm proceeds in the following way:

- use the Neutrino Solver to calculate the corresponding minimum distance $D_{\nu,\mathrm{min}}$;
- if the Neutrino Solver yields no solution, this jet assignment is discarded;
- if instead both b-jet candidates have solutions for neutrino momentum, a likelihood discriminant is constructed using the minimum distance $D_{\nu,\mathrm{min}}$ and the invariant mass $m_{\mathrm{t_h}}$ of the two jets hypothesized to belong to the hadronic top decay. We choose the jet assignment with the lowest value of the negative log likelihood $-\ln(\lambda_3)$ (label 3 refers to the requirement of three jets):

$$-\ln(\lambda_3) = -\ln(P_{\mathrm{m_{t_h}}}) - \ln(P_\nu(D_{\nu,\mathrm{min}})), \quad (2)$$

where $P_\nu(D_{\nu,\mathrm{min}})$, shown in Fig. 3 upper left, is the probability to correctly identify b_ℓ using $D_{\nu,\mathrm{min}}$; $P_{\mathrm{m_{t_h}}}$, shown in Fig. 3 upper right, is the probability of the invariant mass of the hypothesized $\mathrm{b_h}$ and the jet from W boson decay. The distribution of $-\ln(\lambda_3)$ is shown in the lower plot of Fig. 3. Jet assignments with values of $-\ln(\lambda_3) > 13$ are discarded to improve the signal to background ratio.

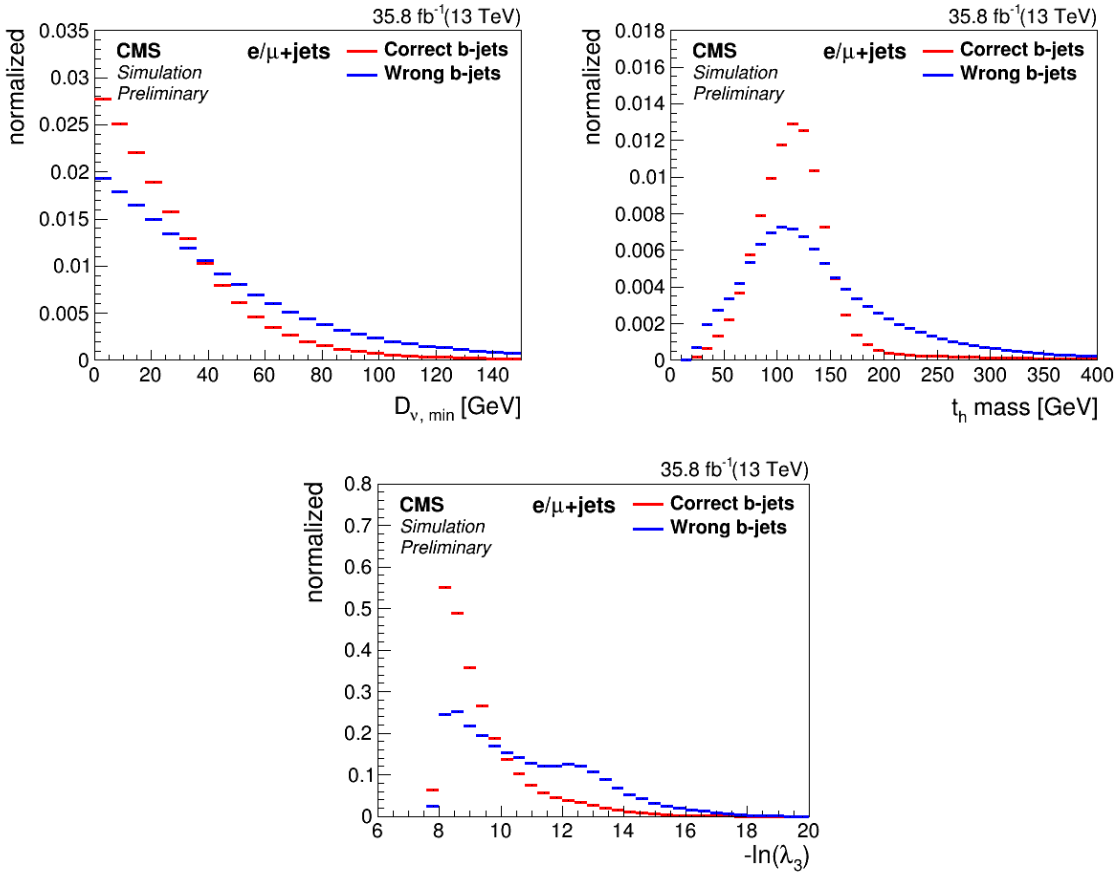

Figure 3: Three-jet reconstruction. Upper left: normalized distributions of the distance $D_{\nu,\mathrm{min}}$ for correctly and wrongly selected b_ℓ candidates. Upper right: normalized mass distribution of the correctly and wrongly selected b_h and the jet from W. Lower plot: Distribution of the negative combined log-likelihood.

When the top candidate is off-shell, no solution can be found in the mass constraints and we continue with the next b jet candidate. In this case, the algorithm is not able to assign b jets correctly. Overall, this algorithm identifies the correct b jet assignment in 80% of three jet events.

Leptonic top quark decays are fully reconstructible, regardless of whether we have three or four jets. The hadronically decaying top quark candidate in the missing jet category is approximated by the system of two jets identified to be associated with the hadronic top quark decay. Figure 4 shows the resolutions of the invariant mass of the $\mathrm{t\bar{t}}$ system and the difference in rapidity for three jet events, compared to those with at least four jets. It is worth noting that only the widths of these distributions are important, since the respective templates are derived separately for different jet multiplicity bins. The resolution shows that the three jet reconstruction is competitive with the one achieved in the four jet category.

To summarize, the newly developed three-jet reconstruction algorithm allows us to increase the yields in the sensitive low $M_{\mathrm{t\bar{t}}}$ region. As will be shown in Sec. 9, the addition of three-jet events also helps to reduce the systematic uncertainty due to sources that cause migration between jet multiplicity bins, e.g. jet energy scale variation and the hadronization model.

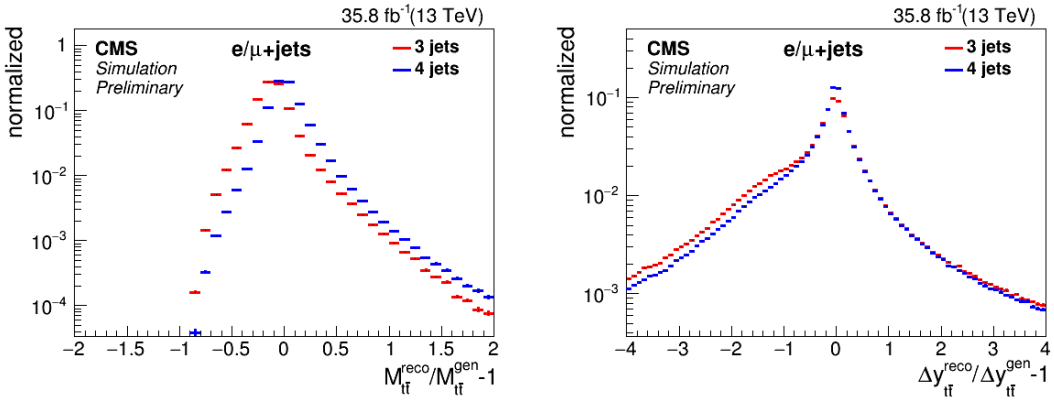

Figure 4: Resolution of the invariant mass of the $t\bar{t}$ system (left) and the difference in rapidity of top quark/antiquark (right) for three-jet and at least four-jet event categories.

6 Background estimation

Backgrounds in this analysis arise from QCD multijet production, single top quark production, and vector boson production in association with jets (V+jets). The expected number of events from WW and WZ production is negligible and we ignore it in the signal region (SR).

The contribution from single top quark and V+jets are estimated from the simulated samples. Due to the reduced size of the QCD multijet samples after selection, we derive smoother distributions of $M_{t\bar{t}}$ and $\Delta y_{t\bar{t}}$ from a control region. Events in the control region (CR) are selected in the same way as the signal events, except that the maximum value of the CSV discriminator of jets in each event has to be less than 0.6. Hence events in the CR originate predominately from V+jets and QCD multijet processes. We take the distribution for $M_{t\bar{t}}$ and $\Delta y_{t\bar{t}}$ from the data in the CR, subtracting the expected contribution from the residual V+jets, single top quark, $t\bar{t}$, and WW and WZ processes. The distributions are then normalized by the ratio of the number of events in the SR (N^{SR}_{QCDMC}) and CR (N^{CR}_{QCDMC}) determined from multijet simulated events:

$$N^{SR}_{QCD} = N^{CR}_{resDATA} \times \frac{N^{SR}_{QCDMC}}{N^{CR}_{QCDMC}}, \tag{3}$$

where $N^{CR}_{resDATA}$ is the residual yield in data (data minus the non-QCD components). The normalization uncertainty is estimated to be 30%. The shape uncertainty due to the CR definition is evaluated selecting events, where the lepton fails the isolation requirement. The uncertainty is defined by the difference between the distributions of events that pass or fail the value of CSV requirement, and can be as large as 60% in some regions of phase space.

7 Event yields and control plots

Table 1 shows the event yields with the statistical uncertainties after event selection and $t\bar{t}$ reconstruction. All of the $t\bar{t}$ components depend on the top quark Yukawa coupling from the production, so all of them are considered as signal. Here, the signal simulation is divided into the following categories: correctly reconstructed $t\bar{t}$ systems ($t\bar{t}$ right reco), events where all decay products are available, but the algorithm failed to identify the correct jet assignments ($t\bar{t}$ wrong reco), ℓ+jets $t\bar{t}$ events where at least one decay product is missing ($t\bar{t}$ not reconstructible), and $t\bar{t}$ events from dileptonic or fully hadronic decays ($t\bar{t}$ background).

Table 1: Expected and observed yields with statistical uncertainties after event selection. Events are categorized in the $\mathrm{t\bar{t}}$ simulation as: correctly identified $\mathrm{t\bar{t}}$ systems ($\mathrm{t\bar{t}}$ right); events where all decay products are available, but the $\mathrm{t\bar{t}}$ reconstruction algorithm did not identify the correct $\mathrm{t\bar{t}}$ permutation ($\mathrm{t\bar{t}}$ wrong); non-reconstructible events where the algorithm failed to identify at least one top candidate ($\mathrm{t\bar{t}}$ not reco); and events arising from the dileptonic or fully hadronic $\mathrm{t\bar{t}}$ channels ($\mathrm{t\bar{t}}$ background).

Source	3 jets	4 jets	$\geq$5 jets
$\mathrm{t\bar{t}}$ right reco	130 523±154	92 895±130	71 643±114
$\mathrm{t\bar{t}}$ wrong reco	29 298±73	17 356±57	43 073±89
$\mathrm{t\bar{t}}$ not reco	50 695±96	88 763±127	80 960±122
$\mathrm{t\bar{t}}$ background	53 465±99	26 085±69	25 047±68
single t	17 849±40	6922±27	6294±26
V+jets	8990±100	2824±52	2478±49
QCD multijet	19 835±6 247	2100±603	1083±210
Expected sum	310 653±254	236 945±212	230 574±211
Observed data	308 932±556	237 491±487	226 788±476

Figures 5–7 show the comparison of data to simulation in the missing transverse momentum, the pseudorapidity of the lepton, and several kinematic variables of the top quark and $\mathrm{t\bar{t}}$ system. The distributions for QCD multijet backgrounds are derived from the data CR, described in Sec. 6. In general, good agreement between data and prediction is observed.

8 Statistical treatment

Two-dimensional data distributions in ($M_{\mathrm{t\bar{t}}}$, $\Delta y_{\mathrm{t\bar{t}}}$) are fit to the sum of the predicted contributions to infer the value of Y_{t} for events with three, four, and five or more jets in the final state. There are three bins in $|\Delta y_{\mathrm{t\bar{t}}}|$: 0 – 0.6, 0.6 – 1.2, and 1.2 or above. A minimum of 10 000 simulated events are required in each bin of $M_{\mathrm{t\bar{t}}}$ and $|\Delta y_{\mathrm{t\bar{t}}}|$. This results in a first $M_{\mathrm{t\bar{t}}}$ bin range of 0 – 300 GeV, 0 – 340 GeV, and 0 – 400 GeV for $|\Delta y_{\mathrm{t\bar{t}}}|$: 0 – 0.6, 0.6 – 1.2, and 1.2 or above, respectively. Under these conditions, there are 21, 17, and 17 bins for event categories with three, four, and five or more jets, respectively. The $M_{\mathrm{t\bar{t}}}$ binning is labeled in the axis of the event distributions in Fig. 10.

The bin limits are selected to capture the different behavior of the EW correction, as seen in different regions of Fig. 2. For example, the corrections for $|\Delta y_{\mathrm{t\bar{t}}}| > 1.2$ differ significantly, depending on Y_{t}, and similarly for $M_{\mathrm{t\bar{t}}} > 500$ GeV. The likelihood model is constructed as a product of Poisson likelihoods [31, 32] for the observed number of events, $n_{\mathrm{obs}}^{\mathrm{bin}}$ in each ($M_{\mathrm{t\bar{t}}}$, $|\Delta y_{\mathrm{t\bar{t}}}|$) bin:

$$\mathcal{L} = \prod_{\mathrm{bin}\,\in(M_{\mathrm{t\bar{t}}},|\Delta y_{\mathrm{t\bar{t}}}|)} \mathcal{L}_{\mathrm{bin}} = \prod_{\mathrm{bin}} \mathrm{Pois}(n_{\mathrm{obs}}^{\mathrm{bin}} | s^{\mathrm{bin}}(\theta) \times R^{\mathrm{bin}}(Y_{\mathrm{t}}) + b^{\mathrm{bin}}(\theta)) \times \rho(\theta|\tilde{\theta}), \tag{4}$$

where s^{bin} is the POWHEG prediction for number of $\mathrm{t\bar{t}}$ events; b^{bin} is the prediction for the number of events due to each background process (single top quark, V+jets and multijet production), $R^{\mathrm{bin}}(Y_{\mathrm{t}}) = s^{\mathrm{bin}}(Y_{\mathrm{t}})/s^{\mathrm{bin}}(\mathrm{POWHEG})$ encodes the effect of different Y_{t} coupling scenarios, parametrized with a quadratic dependence on Y_{t} in each bin (shown in Figs. 8 and 9 for the first $|\Delta y_{\mathrm{t\bar{t}}}|$ bin), and θ represents the full suite of nuisance parameters with $\rho(\theta|\tilde{\theta})$ described by Gaussian distributions parametrizing the uncertainty on their true values $\tilde{\theta}$. The different sources of systematic uncertainties are described in detail in Sec. 9. The quantity $R^{\mathrm{bin}}(Y_{\mathrm{t}})$ is

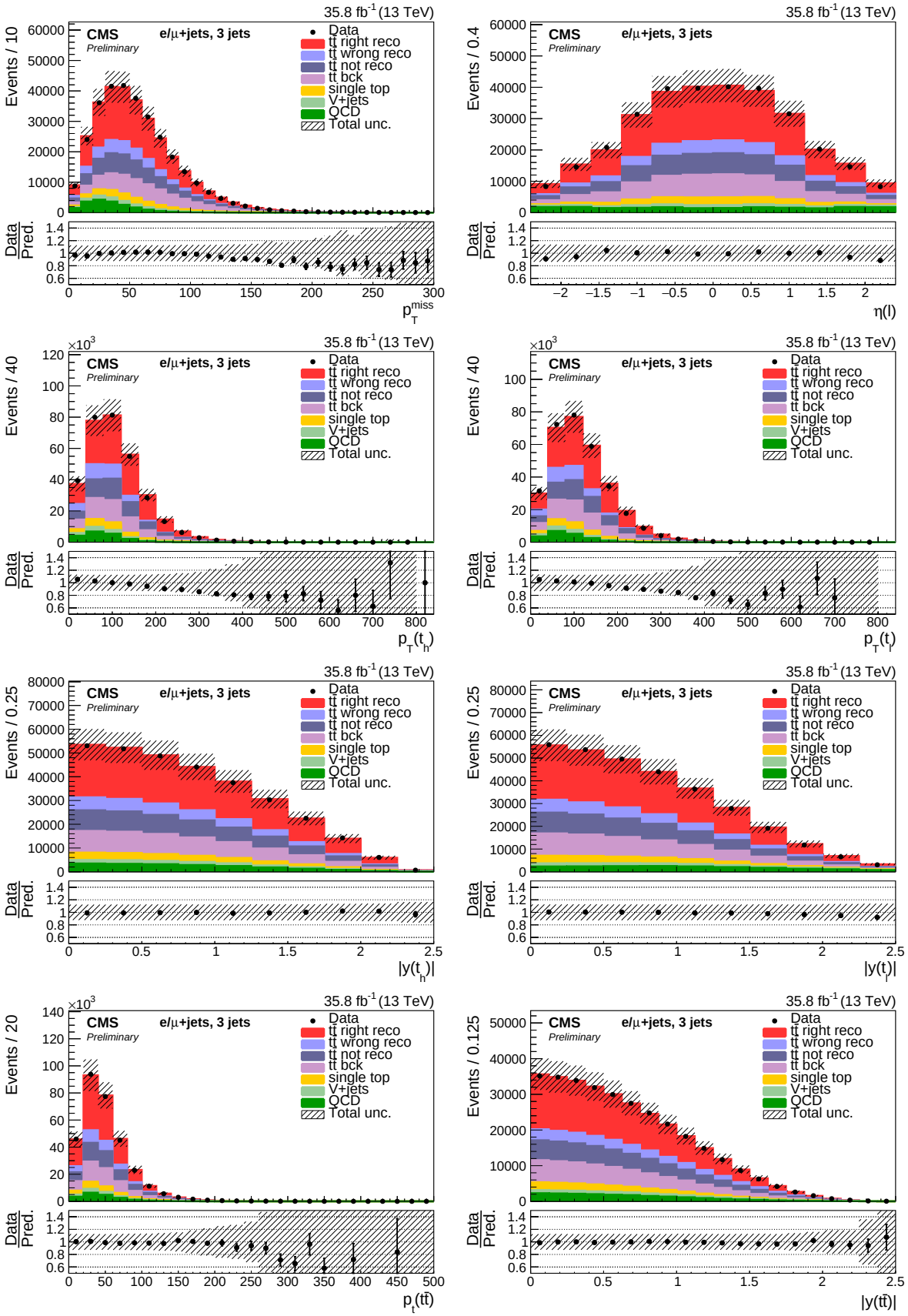

Figure 5: Three-jet events after selection and $\mathrm{t\bar{t}}$ reconstruction. The plots show the missing transverse momentum ($p_{\mathrm{T}}^{\mathrm{miss}}$), the lepton pseudorapidity, and p_{T} and absolute rapidity y of leptonic top quark, hadronic top quark, and the $\mathrm{t\bar{t}}$ system. The hatched band shows the total uncertainty associated with signal and background predictions with the sources of uncertainty uncorrelated and summed in quadrature. The ratios of data to the sum of the predicted yields are provided at the bottom of each panel.

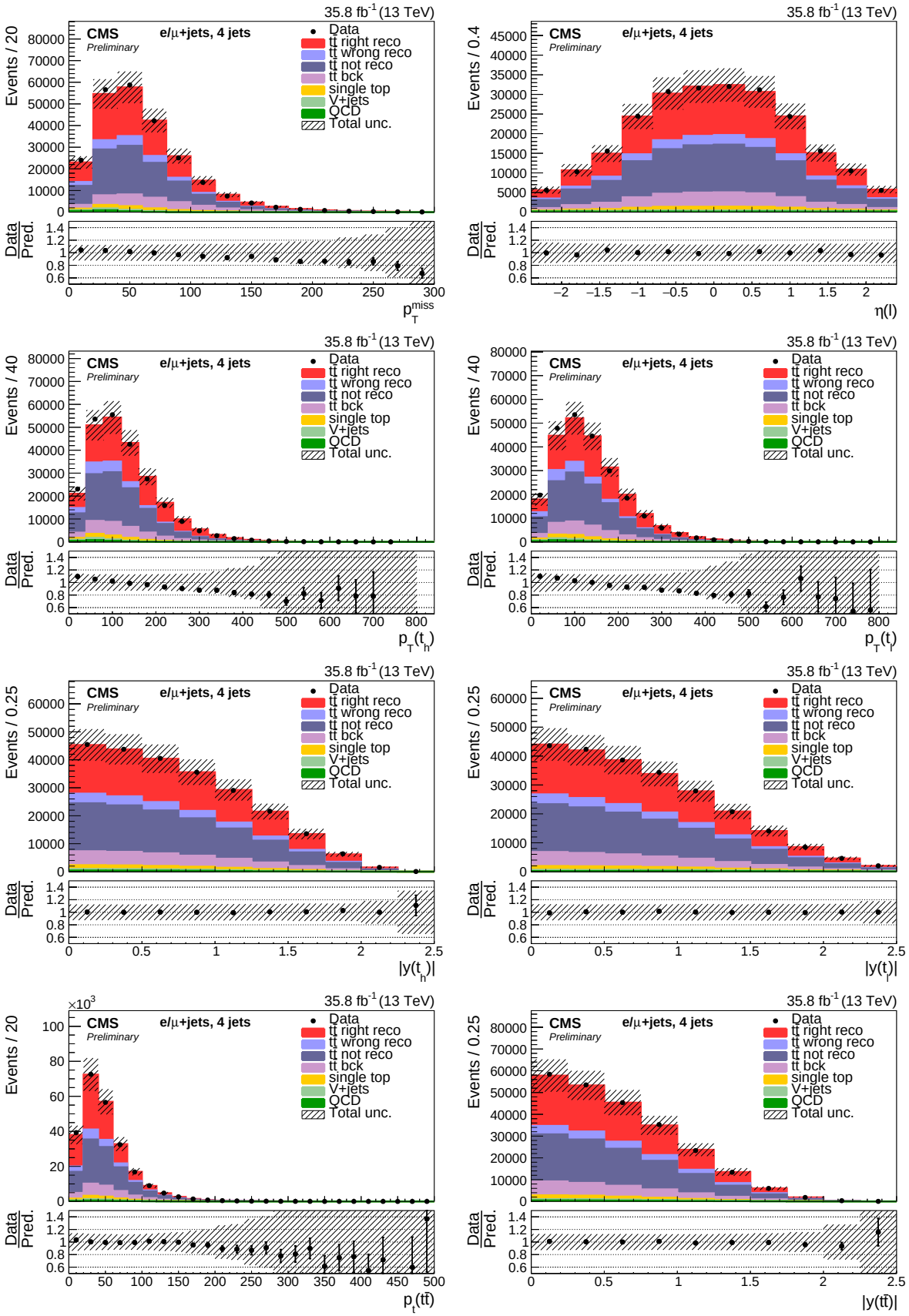

Figure 6: Four-jet events after selection and $t\bar{t}$ reconstruction. Same plots as described in Fig. 5.

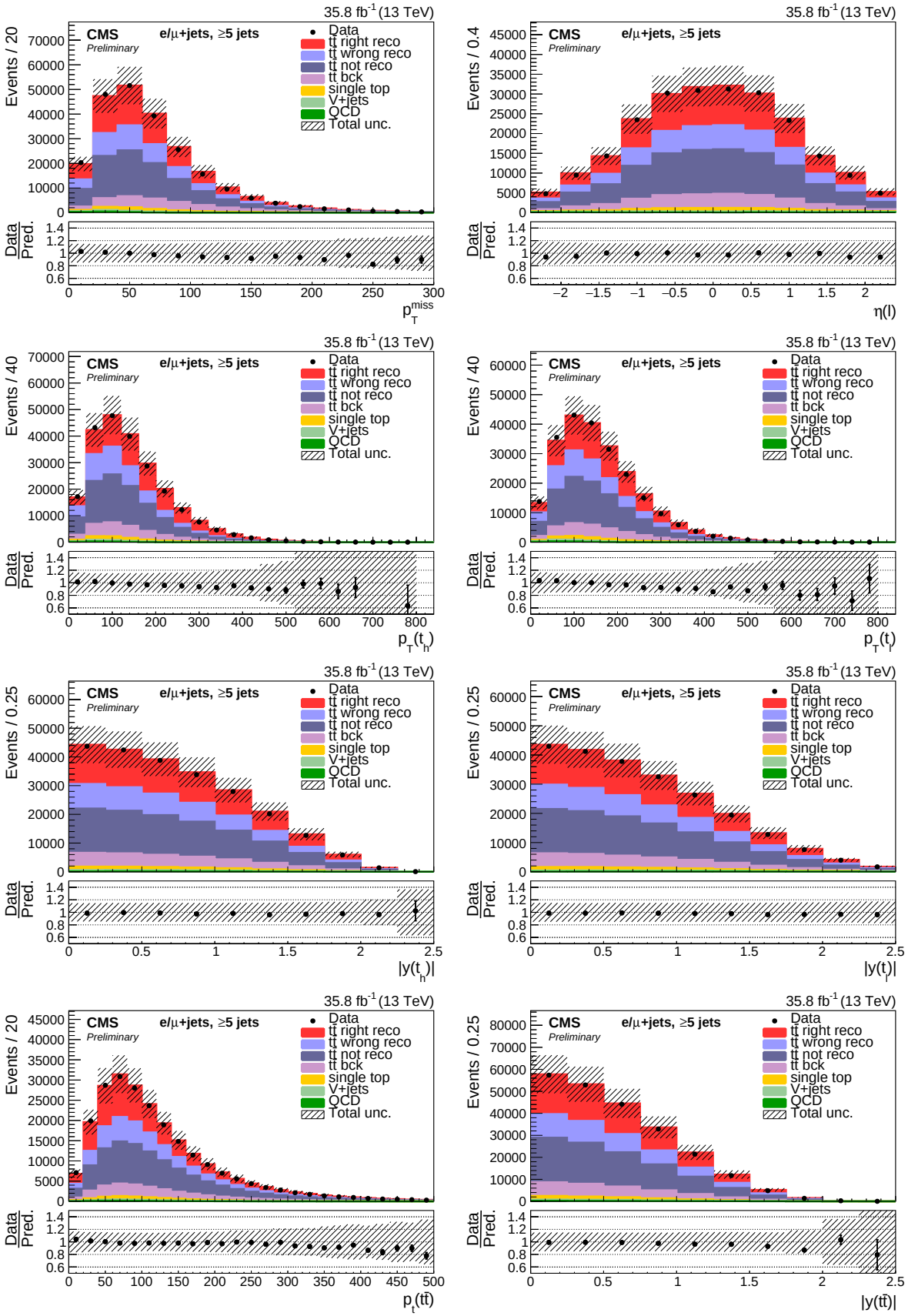

Figure 7: Events with five or more jets after selection and $t\bar{t}$ reconstruction. Same plots as described in Fig. 5.

the main parameter of interest in the fit, as it represents the strength of the EW correction over the uncorrected POWHEG yields. The strength $R(Y_t) = 1$ corresponds to the SM top Yukawa coupling prediction.

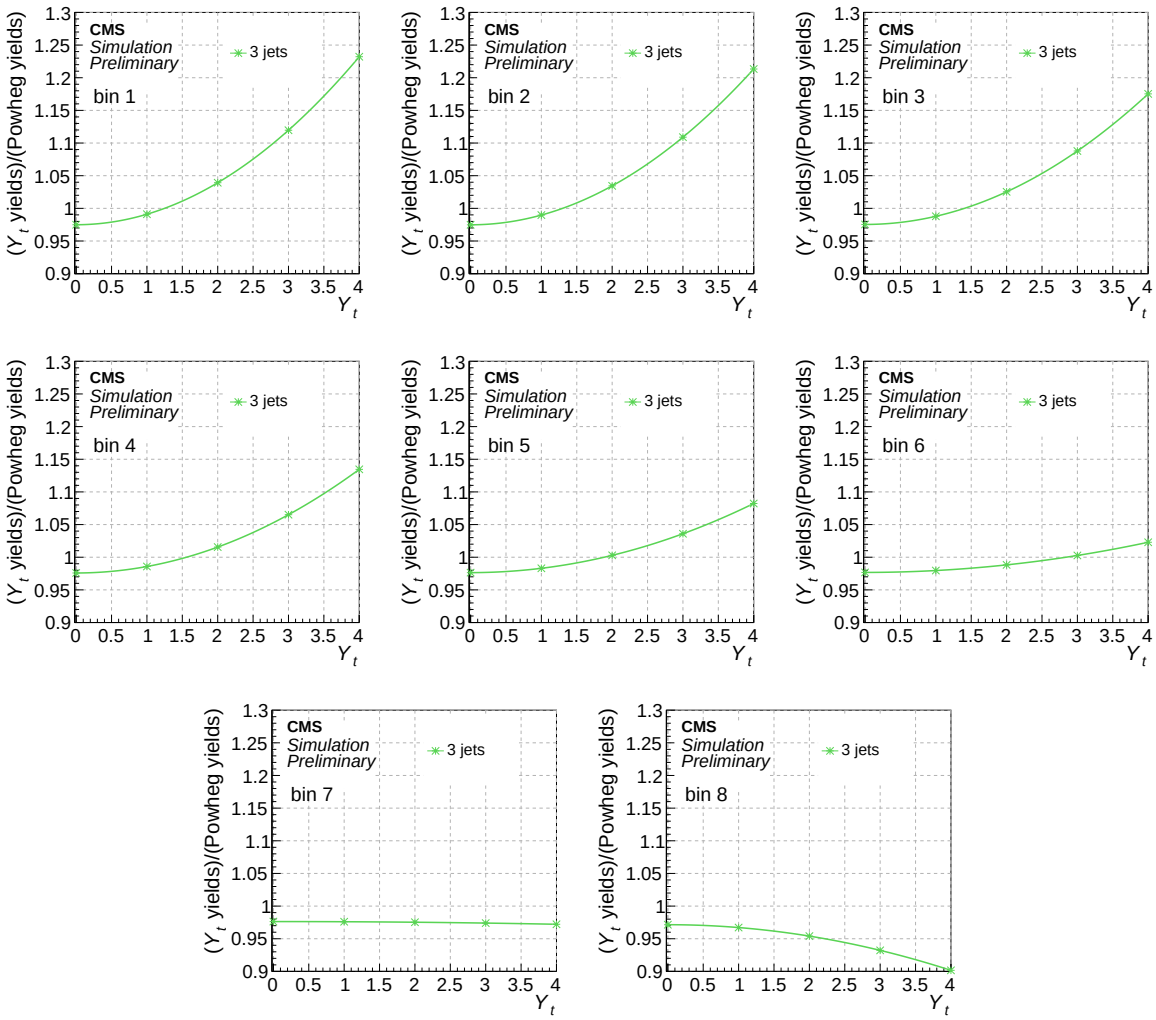

Figure 8: The strength of the EW correction, relative to the POWHEG expected signal, $R^{\text{bin}}(Y_t)$, as a function of Y_t in the three-jet category. Each plot corresponds to one of the eight $M_{t\bar{t}}$ bins for $|\Delta y_{t\bar{t}}| < 0.6$ (see Fig. 10). A quadratic fit is performed in each bin.

9 Systematic uncertainties

We describe here the different sources of experimental and theoretical uncertainties and their effect on determining Y_t. Systematic uncertainties which do not alter the shape of the distributions of $M_{t\bar{t}}$ and $\Delta y_{t\bar{t}}$ are treated as normalization uncertainties, while others are treated as shape uncertainties. Their effect is evaluated bin-by-bin in the likelihood. Table 2 lists all the systematic uncertainties.

The uncertainty in the integrated luminosity is 2.5% [33]. The simulation samples are reweighted to match the measured data distribution in the number of collisions per events. The uncertainty on the total inelastic pp cross section, which affects the pileup estimate, is estimated by varying the average number of pileup events per bunch crossing by 5%.

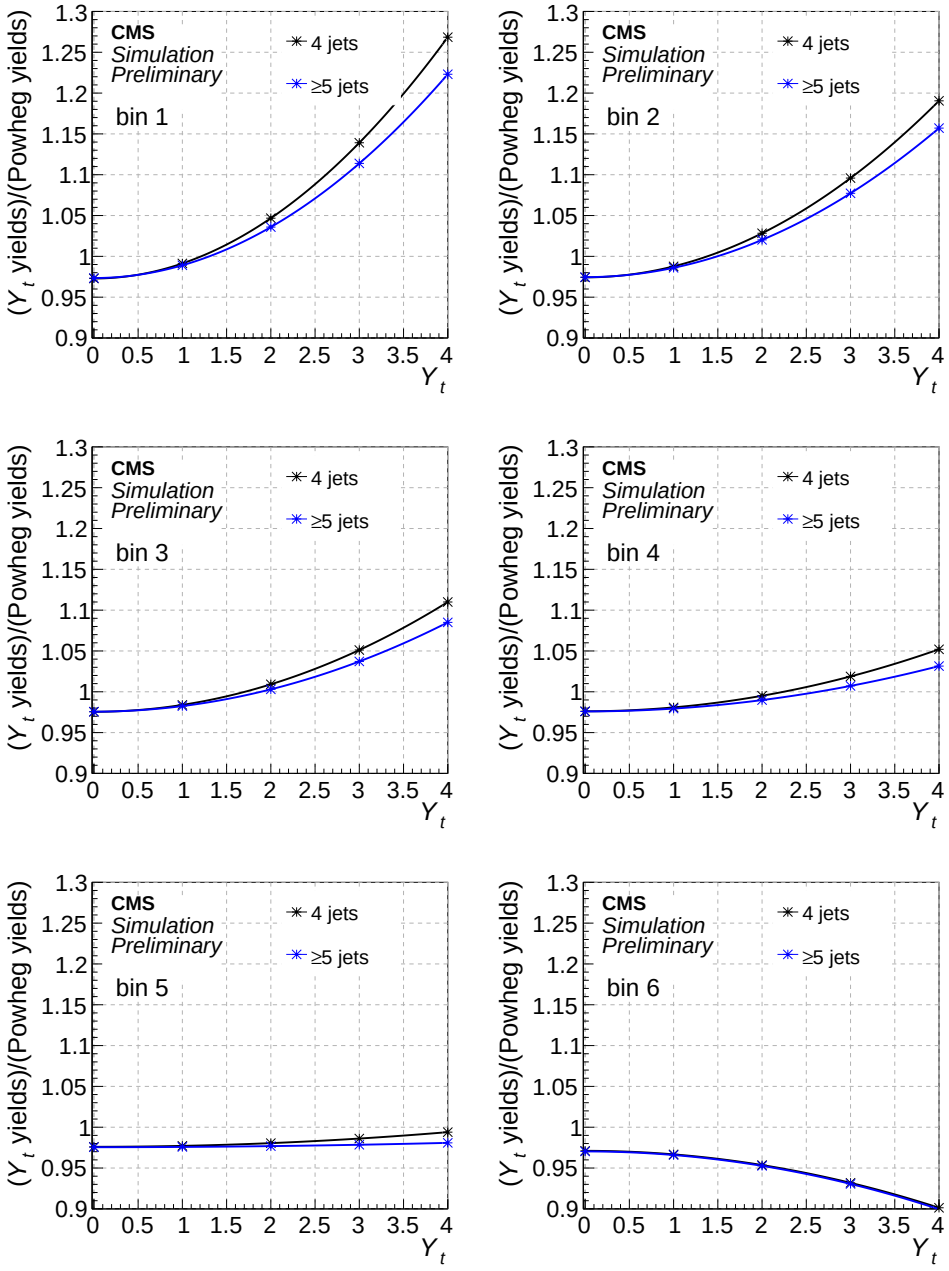

Figure 9: The strength of the EW correction, relative to the POWHEG expected signal, $R^{\text{bin}}(Y_t)$, as a function of Y_t in the categories with four and five or more jets. Each plot corresponds to one of the six $M_{t\bar{t}}$ bins for $|\Delta y_{t\bar{t}}| < 0.6$ (see Fig. 10). A quadratic fit is performed in each bin.

Lepton efficiency scale factors, which account for differences in the trigger, reconstruction, and identification efficiencies between data and simulation, are measured using a tag-and-probe method in $Z \to \ell^+\ell^-$ events [34, 35]. These efficiencies are measured in bins of lepton p_T, η, and jet multiplicities, and then applied to the simulations to match the data. The overall uncertainty on the final measurement from these lepton scale factors is approximately 2%.

Uncertainties in the jet energy calibration (JEC) are evaluated by shifting the energies of jets in the simulation up and down by one standard derivation in bins of p_T and η. According to the different sources of JEC uncertainties and the jet flavors, a total of 19 shape variations are considered. The uncertainty in the jet energy resolution (JER) is calculated by broadening the resolution in simulation and recomputing the acceptances [25], for which the resulting effect is a change of less than 1% in event yields. The b tagging efficiency in simulation is corrected using scale factors determined from efficiencies measured in data and simulation [26]. The uncertainty in the measured scale factors ranges between 1 to 20% per jet, leading to an overall effect on the final measurement of 2 – 3%.

The single top quark background estimate is affected by 15% normalization uncertainties due to the experimental cross section, estimated by the combined results of t-channel and Wt production [36]. Similarly estimated, normalization uncertainty for V+jet background is 30% , based on the uncertainty of the W +heavy flavor production cross section [37]. The variations from all the other sources of systematic uncertainties such as scale factors are considered as well. The QCD multijet data-based estimates include a 30% normalization uncertainty for Eq. 3, and a shape difference observed between different control region definitions (described in Sec. 6). The uncertainty from p_T^{miss}due to the electron, muon, and unclustered energy uncertainties, result in a negligible effect on the acceptance. All the major experimental uncertainties described above are evaluated for each process in all reconstruction channels.

Uncertainties in the renormalization and factorization scales affect the number of events expected in our simulated samples. These uncertainties are evaluated by varying each scale independently by a factor of 2. We consider separate variations of the renormalization and factorization scales by taking the envelope of the observed variations as the quoted uncertainty. To account for possible correlation between the two sources of uncertainty, we also add an additional shape nuisance parameter that corresponds to the same-side variation of both parameters. The different replicas in the NNPDF3.0 PDF set [15] are used to estimate the corresponding uncertainty in the shape from the changed acceptance in each bin, which amounts to a combined variation as large as 5%. The different replicas due to the variation of strong coupling constant α_S results in changes of the acceptance of around 1%.

The uncertainty due to the top quark mass measurement is estimated by taking the acceptance variations in simulations generated with m_t varied by ± 1 GeV, and it results in a shape variation as large as 7%. The dependence of $M_{t\bar{t}}$ and $\Delta y_{t\bar{t}}$ on the correct description of the top quark p_T in the simulation is taken into account by checking the difference in acceptance when the nominal POWHEG NLO samples are scaled to match the average top quark p_T distributions calculated in Ref. [38] at NNLO in α_s (up to 6% difference with the nominal top p_T). This uncertainty is treated as a shape nuisance parameter in the likelihood for the $t\bar{t}$ samples.

In the following, we describe the sources of uncertainties due to modelling the parton shower. The uncertainty in matching the matrix element calculation to the parton shower is estimated by changing the parameter that regulates the damping of real emission in the NLO calculation [39], resulting in an effect of around 1 – 5%. The scales, which determine initial- (ISR) and final-state radiation (FSR) are also varied [14], resulting in a maximum change of 4% in the acceptance and shape variations as large as 10%. The uncertainty resulting from the model-

ing of the amount of multiple-parton interactions per event [39] is estimated using dedicated samples, where the number of underlying events is varied up and down in the PYTHIA8 tune, and is found to have a negligible effect on the result. Color reconnection reconfigures color strings after the parton shower, affecting the W boson decays [39]. This source of uncertainty typically results in shape differences smaller than 1%. The uncertainty in b-quark fragmentation, the momentum transfer from the b quark to the B hadron, is estimated by varying the parametrized function in the PYTHIA8 simulation. It can produce a shape variation as large as 8%. The branching fraction of B hadrons decaying semileptonically may change the b jet energy response and, therefore, the uncertainty is calculated by reweighting the simulation with one standard variation of the measurement [40]. It makes an effect on the acceptance as large as 3%.

Finally, the EW correction is implemented by reweighting nominal POWHEG samples with the ratio of weak correction over the LO cross section calculated by HATHOR. As recommended by the HATHOR authors [41], the associated systematic uncertainty for this procedure can be estimated from the difference between the multiplicative and additive treatments, i.e. $(1 + \delta_{\mathrm{QCD}})(1 + \delta_{\mathrm{EW}})$ and $(1 + \delta_{\mathrm{QCD}} + \delta_{\mathrm{EW}})$, where δ_{QCD} is estimated from the effect of varying the factorization and renormalization scale up and down on the NLO cross section, and δ_{EW} is the ratio of weak correction over the LO cross section obtained from HATHOR. The difference is $\delta_{\mathrm{QCD}} \times \delta_{\mathrm{EW}}$, which is also a function of Y_{t} since the overall effect of weak correction increases for increasing Yukawa couplings. This uncertainty is accounted for as a shape nuisance in the likelihood fit.

Experimental uncertainties are treated as 100% correlated among signal and background processes and across jet multiplicity channels.

10 Results

As described in Sec. 5, the data events are analyzed in three exclusive channels according to the number of jets in the final state. The expected signal and background estimation shown in Table 1 and the systematic uncertainties described in Sec. 9 are used to construct a binned likelihood function (Eq. 4) as a product of Poisson probabilities from all bins in ($M_{\mathrm{t\bar{t}}}$,$\Delta y_{\mathrm{t\bar{t}}}$). From this, we construct a profile likelihood ratio test-statistic $q(Y_{\mathrm{t}}) = -2\ \ln\left[\mathcal{L}(Y_{\mathrm{t}}, \hat{\hat{\theta}}) / \mathcal{L}(\hat{Y}_{\mathrm{t}}, \hat{\theta})\right]$, where $\hat{\hat{\theta}}$ in the numerator denotes the value of the estimator $\hat{\theta}$ that maximizes the likelihood for a specific Y_{t}, i.e., it is the conditional maximum-likelihood estimator of θ (and thus is a function of Y_{t}). The denominator is the maximized (unconditional) likelihood function, i.e., $\hat{Y}_{\mathrm{t}}$ and $\hat{\theta}$ are the values of the estimators that simultaneously maximize the likelihood. The statistical procedure to extract the parameter of interest is detailed in Ref. [42]. The distributions of $M_{\mathrm{t\bar{t}}}$ and $\Delta y_{\mathrm{t\bar{t}}}$ after performing the likelihood fit are shown in Fig. 10.

We set a limit on the top quark Yukawa coupling by scanning the likelihood with respect to Y_{t}. The limits on Y_{t} are reported at the 95% confidence level (CL) where the value of the test-statistic is 3.84. The likelihood scan distributions can be found in Fig. 11. The expected and the observed limits are presented in Table 3.

11 Summary

A limit on the top quark Yukawa coupling is presented, extracted by investigating top lepton+jets decays into a muon or electron and several jets in 35.8 fb^{-1} of CMS data at $\sqrt{s}$ = 13 TeV. The $\mathrm{t\bar{t}}$ production rate is sensitive to the top quark Yukawa coupling through electroweak cor-

Table 2: Summary of the sources of systematic uncertainties, their effects and magnitudes on signal and backgrounds. If the uncertainty shows a shape dependency on the $M_{t\bar{t}}$ and $\Delta y_{t\bar{t}}$ distributions, it is being considered in the likelihood and labeled as "shape" in the table. For columns with several numbers, the numbers refer to the events with three, four, five and more jets.

Uncertainty	$t\bar{t}$	single t	V+jets	QCD
Luminosity	2.5%	2.5%	2.5%	2.5%
Pileup	shape	shape	-	-
Lepton ID/trigger	shape	shape	shape	-
JEC (19 independent variations)	shape	shape	-	-
JER	shape	-	-	-
b tagging scale factor	shape	shape	shape	-
b-mistag scale factor	shape	shape	shape	-
Background normalization	-	15%	30%	30%
CSV inversion on QCD template	-	-	-	shape
Factorization & renormalization scale	shape	shape	shape	-
PDF	shape	shape	-	-
$\alpha_s(M_Z)$ in PDFs	shape	shape	-	-
Top quark mass	shape	-	-	-
Top quark p_T modeling	shape	-	-	-
Parton Shower				
-NLO shower matching	shape	-	-	-
-ISR	2%/2%/3%	-	-	-
-FSR	shape	shape	-	-
-Color reconnection	shape	-	-	-
-b-jet fragmentation	shape	shape	-	-
-B hadron branching fraction	shape	shape	-	-
Weak correction $\delta_{QCD}\delta_{EW}$	shape	-	-	-

Table 3: The expected and observed 95% CL limits on Y_t.

Channel	Expected 95% CL	Observed 95% CL
3 jets	$Y_t < 2.17$	$Y_t < 2.59$
4 jets	$Y_t < 1.88$	$Y_t < 1.77$
5 jets	$Y_t < 2.03$	$Y_t < 2.23$
Combined	$Y_t < 1.62$	$Y_t < 1.67$

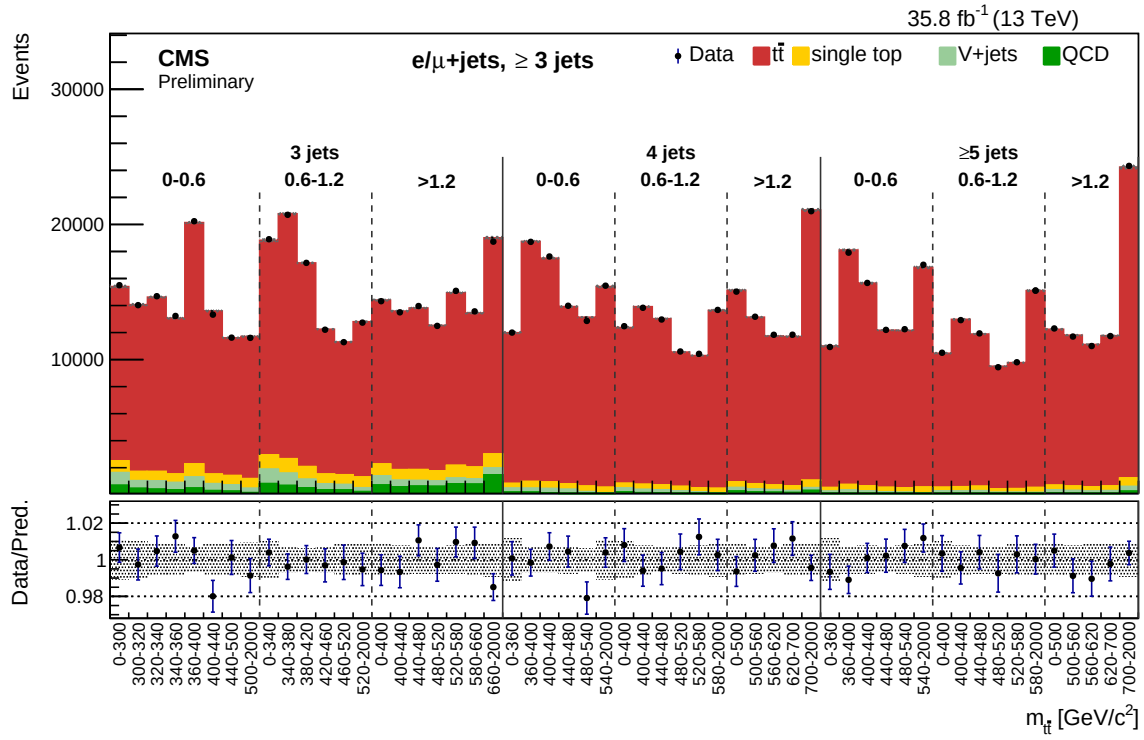

Figure 10: The $M_{t\bar{t}}$ distribution in $|\Delta y_{t\bar{t}}|$ bins for all channels combined, after the likelihood fit. The hatched bands show the total post-fit uncertainty. The ratios of data to the sum of the predicted yields are provided at the bottom of each panel.

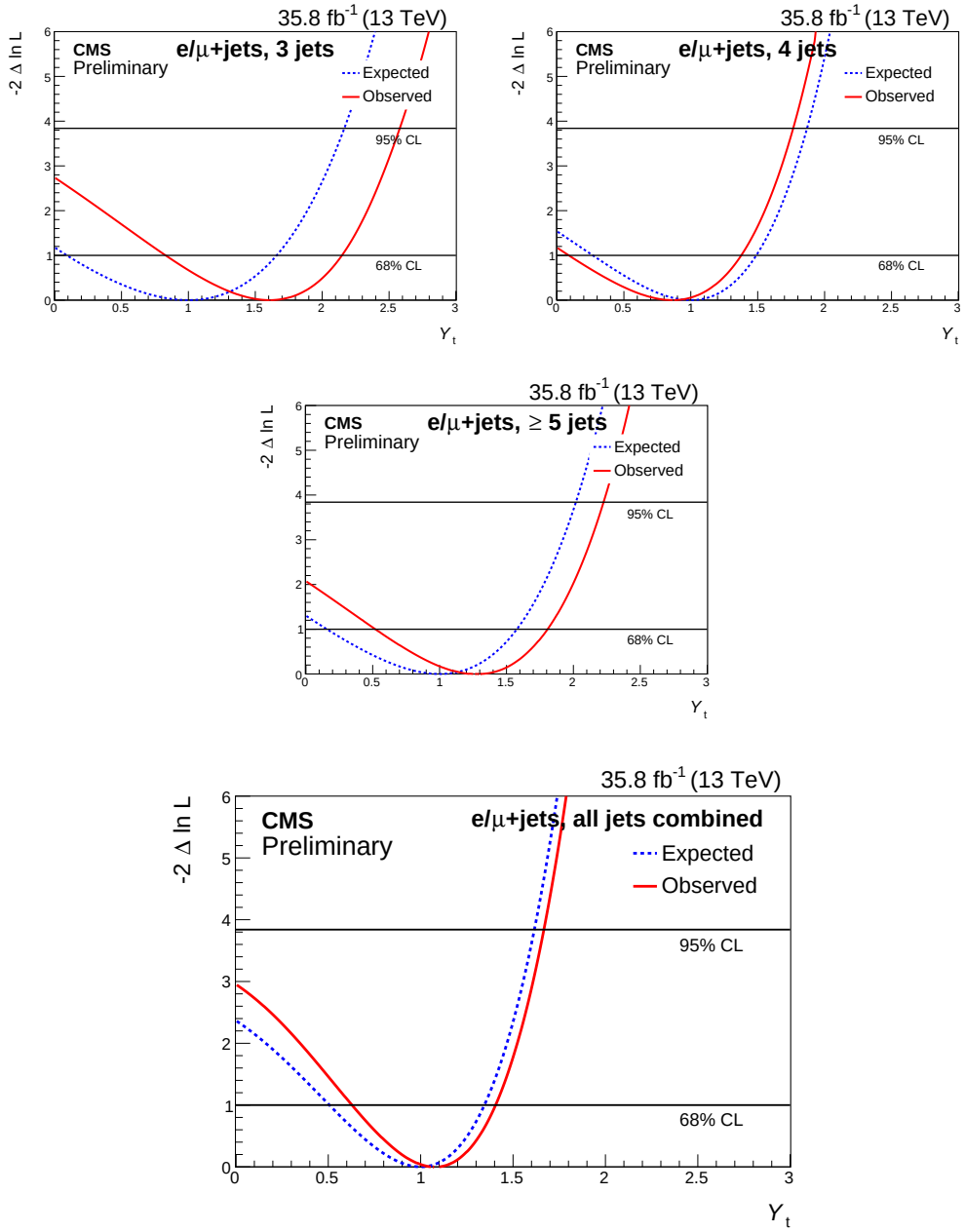

Figure 11: The test-statistic scan versus Y_t for each channel (three jets, four jets, five or more jets), and all channels combined. The test-statistic minimum indicates the best fit of Y_t. The horizontal lines indicate 68% CL and 95% CL.

rections that can modify the distributions of the mass of top quark-antiquark pairs, $M_{t\bar{t}}$, and the rapidity difference between top quarks/antiquarks, $\Delta y_{t\bar{t}}$. Top quark-antiquark pair events have been reconstructed with a novel algorithm applied to events with three or at least four reconstructed jets and two b tags. The inclusion of events where only three jets are reconstructed (one missing jet in the leading order lepton+jets topology) improves the sensitivity of the analysis by including more events from the low $M_{t\bar{t}}$ region, which is most sensitive to the Yukawa coupling. The top quark Yukawa coupling is extracted by comparing the data with the expected $t\bar{t}$ signal for different values of Y_t in a total of 57 bins in $M_{t\bar{t}}$, $\Delta y_{t\bar{t}}$, and the number of reconstructed jets. The value of the top quark Yukawa coupling is constrained to be less than 1.67 at the 95% confidence level.

References

[1] M. Czakon et al., "Top-pair production at the LHC through NNLO QCD and NLO EW", *JHEP* **10** (2017) 186, doi:10.1007/JHEP10(2017)186, arXiv:1705.04105.

[2] M. L. Czakon et al., "Top quark pair production at NNLO+NNLL′ in QCD combined with electroweak corrections", in *11th International Workshop on Top Quark Physics (TOP2018) Bad Neuenahr, Germany, September 16-21, 2018*. 2019. arXiv:1901.08281.

[3] J. H. Kühn, A. Scharf, and P. Uwer, "Weak Interactions in Top-Quark Pair Production at Hadron Colliders: An Update", *Phys. Rev. D* **91** (2015) 014020, doi:10.1103/PhysRevD.91.014020, arXiv:1305.5773.

[4] CMS Collaboration, "Measurement of differential cross sections for top quark pair production using the lepton+jets final state in proton-proton collisions at 13 TeV", *Phys. Rev.* **D95** (2017) 092001, doi:10.1103/PhysRevD.95.092001, arXiv:1610.04191.

[5] M. Aliev et al., "HATHOR: HAdronic Top and Heavy quarks crOss section calculatoR", *Comput. Phys. Commun.* **182** (2011) 1034, doi:10.1016/j.cpc.2010.12.040, arXiv:1007.1327.

[6] CMS Collaboration, "Measurement of differential cross sections for the production of top quark pairs and of additional jets in lepton+jets events from pp collisions at $\sqrt{s} = 13$ TeV", *Phys. Rev.* **D97** (2018) 112003, doi:10.1103/PhysRevD.97.112003, arXiv:1803.08856.

[7] W. Beenakker et al., "Electroweak one loop contributions to top pair production in hadron colliders", *Nucl. Phys.* **B411** (1994) 343, doi:10.1016/0550-3213(94)90454-5.

[8] P. Nason, "A new method for combining NLO QCD with shower Monte Carlo algorithms", *JHEP* **11** (2004) 040, doi:10.1088/1126-6708/2004/11/040, arXiv:hep-ph/0409146.

[9] S. Frixione, P. Nason, and C. Oleari, "Matching NLO QCD computations with Parton Shower simulations: the POWHEG method", *JHEP* **11** (2007) 070, doi:10.1088/1126-6708/2007/11/070, arXiv:0709.2092.

[10] S. Alioli, P. Nason, C. Oleari, and E. Re, "A general framework for implementing NLO calculations in shower Monte Carlo programs: the POWHEG BOX", *JHEP* **06** (2010) 043, doi:10.1007/JHEP06(2010)043, arXiv:1002.2581.

[11] J. M. Campbell, R. K. Ellis, P. Nason, and E. Re, "Top-pair production and decay at NLO matched with parton showers", *JHEP* **04** (2015) 114, doi:10.1007/JHEP04(2015)114, arXiv:1412.1828.

[12] T. Sjöstrand, S. Mrenna, and P. Skands, "PYTHIA 6.4 physics and manual", *JHEP* **05** (2006) 026, doi:10.1088/1126-6708/2006/05/026, arXiv:hep-ph/0603175.

[13] T. Sjöstrand, S. Mrenna, and P. Z. Skands, "A Brief Introduction to PYTHIA 8.1", *Comput. Phys. Commun.* **178** (2008) 852, doi:10.1016/j.cpc.2008.01.036, arXiv:0710.3820.

[14] P. Skands, S. Carrazza, and J. Rojo, "Tuning PYTHIA 8.1: the Monash 2013 Tune", *Eur. Phys. J. C* **74** (2014) 3024, doi:10.1140/epjc/s10052-014-3024-y, arXiv:1404.5630.

[15] NNPDF Collaboration, "Parton distributions for the LHC Run II", *JHEP* **04** (2015) 040, doi:10.1007/JHEP04(2015)040, arXiv:1410.8849.

[16] M. Czakon and A. Mitov, "Top++: A Program for the Calculation of the Top-Pair Cross-Section at Hadron Colliders", *Comput. Phys. Commun.* **185** (2014) 2930, doi:10.1016/j.cpc.2014.06.021, arXiv:1112.5675.

[17] J. Alwall et al., "The automated computation of tree-level and next-to-leading order differential cross sections, and their matching to parton shower simulations", *JHEP* **07** (2014) 079, doi:10.1007/JHEP07(2014)079, arXiv:1405.0301.

[18] Y. Li and F. Petriello, "Combining QCD and electroweak corrections to dilepton production in FEWZ", *Phys. Rev. D* **86** (2012) 094034, doi:10.1103/PhysRevD.86.094034, arXiv:1208.5967.

[19] P. Kant et al., "HATHOR for single top-quark production: Updated predictions and uncertainty estimates for single top-quark production in hadronic collisions", *Comput. Phys. Commun.* **191** (2015) 74, doi:10.1016/j.cpc.2015.02.001, arXiv:1406.4403.

[20] N. Kidonakis, "NNLL threshold resummation for top-pair and single-top production", *Phys. Part. Nucl.* **45** (2014) 714, doi:10.1134/S1063779614040091, arXiv:1210.7813.

[21] J. Allison et al., "Geant4 developments and applications", *IEEE Trans. Nucl. Sci.* **53** (2006) 270, doi:10.1109/TNS.2006.869826.

[22] M. Cacciari, G. P. Salam, and G. Soyez, "The anti-k_t jet clustering algorithm", *Journal of High Energy Physics* **2008** (2008) 063.

[23] M. Cacciari, G. P. Salam, and G. Soyez, "Fastjet user manual", *The European Physical Journal C* **72** (2012), no. 3, 1896, doi:10.1140/epjc/s10052-012-1896-2.

[24] T. C. collaboration, "Determination of jet energy calibration and transverse momentum resolution in CMS", *JINST* **6** (2011) P11002.

[25] CMS Collaboration, "Jet energy scale and resolution in the CMS experiment in pp collisions at 8 TeV", *JINST* **12** (2017) P02014, doi:10.1088/1748-0221/12/02/P02014, arXiv:1607.03663.

[26] CMS Collaboration, "Identification of b quark jets at the CMS Experiment in the LHC Run 2", CMS Physics Analysis Summary CMS-PAS-BTV-15-001, 2016.

[27] CMS Collaboration Collaboration, "Identification of b quark jets at the CMS Experiment in the LHC Run 2", Technical Report CMS-PAS-BTV-15-001, CERN, 2016.

[28] CMS Collaboration, "Measurement of inclusive W and Z boson production cross sections in pp collisions at $\sqrt{s}$ = 8 TeV", *Phys. Rev. Lett.* **112** (2014) 191802, doi:10.1103/PhysRevLett.112.191802, arXiv:1402.0923.

[29] B. A. Betchart, R. Demina, and A. Harel, "Analytic solutions for neutrino momenta in decay of top quarks", *Nucl. Instrum. Meth. A* **736** (2014) 169, doi:10.1016/j.nima.2013.10.039, arXiv:1305.1878.

[30] R. Demina, A. Harel, and D. Orbaker, "Reconstructing events with one lost jet", *Nuclear Instruments and Methods in Physics Research Section A: Accelerators, Spectrometers, Detectors and Associated Equipment* **788** (2015) 128, doi:https://doi.org/10.1016/j.nima.2015.03.069.

[31] The ATLAS Collaboration, The CMS Collaboration, The LHC Higgs Combination Group Collaboration, "Procedure for the LHC Higgs boson search combination in Summer 2011", Technical Report CMS-NOTE-2011-005. ATL-PHYS-PUB-2011-11, 2011.

[32] "HiggsAnalysis/CombinedLimit v.5.0.4 for ROOT 6 SLC6 release.". https://twiki.cern.ch/twiki/bin/view/SWGuideHiggsAnalysisCombinedLimit.

[33] CMS Collaboration, "CMS Luminosity Measurement for the 2016 Data Taking Period", CMS Physics Analysis Summary CMS-PAS-LUM-17-001, 2017.

[34] "Performance of electron reconstruction and selection with the CMS detector in proton-proton collisions at $\sqrt{s} = 8$ TeV", *JINST* **10** (2015) P06005.

[35] CMS Collaboration, "Performance of the CMS muon detector and muon reconstruction with proton-proton collisions at $\sqrt{s} = 13$ TeV", *JINST* **13** (2018) P06015, doi:10.1088/1748-0221/13/06/P06015, arXiv:1804.04528.

[36] "LHCTopWG Summary Plots". https://twiki.cern.ch/twiki/bin/view/CMS/SWGuideHiggsAnalysisCombinedLimit. Accessed: 2010-09-30.

[37] "LHCTopWG Summary Plots". https://twiki.cern.ch/twiki/bin/view/CMSPublic/%20PhysicsResultsEWK. Accessed: 2010-09-30.

[38] M. Czakon, D. Heymes, and A. Mitov, "fastNLO tables for NNLO top-quark pair differential distributions", arXiv:1704.08551.

[39] CMS Collaboration, "Investigations of the impact of the parton shower tuning in Pythia 8 in the modelling of tt at $\sqrt{s}$ = 8 and 13 TeV", CMS Physics Analysis Summary CMS-PAS-TOP-16-021, 2016.

[40] Particle Data Group Collaboration, "Review of Particle Physics", *Phys. Rev.* **D98** (2018) 030001, doi:10.1103/PhysRevD.98.030001.

[41] "Peter Uwer, private communication during TOP Readiness Meeting on April 28, 2017.".

[42] J. S. Conway, "Incorporating Nuisance Parameters in Likelihoods for Multisource Spectra", in *Proceedings, PHYSTAT 2011 Workshop on Statistical Issues Related to Discovery Claims in Search Experiments and Unfolding, CERN,Geneva, Switzerland 17-20 January 2011*, p. 115. 2011. arXiv:1103.0354. doi:10.5170/CERN-2011-006.115.